

DOE Award No.: DE-FE0028973

**Quarterly Research Performance Progress
Report**

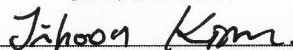
(Period Ending 06/30/2017)

**Advanced Simulation and Experiments of
Strongly Coupled Geomechanics and Flow for
Gas Hydrate Deposits: Validation and Field
Application**

Project Period (10/01/2016 to 09/30/2019)

Submitted by:

Jihoon Kim



Signature

The Harold Vance Department of Petroleum Engineering,
College of Engineering
Texas A&M University
407K Richardson Building
3116 College Station TX, 77843-3136
Email: jihoon.kim@tamu.edu
Phone number: (979) 845-2205

Prepared for:

United States Department of Energy
National Energy Technology Laboratory

June 30, 2017



U.S. DEPARTMENT OF
ENERGY

**NATIONAL ENERGY
TECHNOLOGY LABORATORY**

Office of Fossil Energy

DISCLAIMER

This report was prepared as an account of work sponsored by an agency of the United States Government. Neither the United States Government nor any agency thereof, nor any of their employees, makes any warranty, express or implied, or assumes any legal liability or responsibility for the accuracy, completeness, or usefulness of any information, apparatus, product, or process disclosed, or represents that its use would not infringe privately owned rights. Reference herein to any specific commercial product, process, or service by trade name, trademark, manufacturer, or otherwise does not necessarily constitute or imply its endorsement, recommendation, or favoring by the United States Government or any agency thereof. The views and opinions of authors expressed herein do not necessarily state or reflect those of the United States Government or any agency thereof.

TABLE OF CONTENTS

	<u>Page</u>
DISCLAIMER	2
TABLE OF CONTENTS	3
ACCOMPLISHMENTS	4
Objectives of the project.....	4
Accomplished	4
Task 1	4
Task 2	5
Task 3	12
Task 4	24
Task 5	24
Task 6	26
PRODUCTS	26
BUDGETARY INFORMATION.....	26

ACCOMPLISHMENTS

Objectives of the project

The objectives of the proposed research are (1) to investigate geomechanical responses induced by depressurization experimentally and numerically; (2) to enhance the current numerical simulation technology in order to simulate complex physically coupled processes by depressurization and (3) to perform in-depth numerical analyses of two selected potential production test sites: one based on the deposits observed at the Ulleung basin UBGH2-6 site; and the other based on well-characterized accumulations from the westend Prudhoe Bay. To these ends, the recipient will have the following specific objectives:

1). Information obtained from multi-scale experiments previously conducted at the recipient's research partner (the Korean Institute of Geoscience and Mineral Resources (KIGAM)) that were designed to represent the most promising known Ulleung Basin gas hydrate deposit as drilled at site UBGH2-6 will be evaluated (Task 2). These findings will be further tested by new experimental studies at Lawrence Berkeley National Laboratory (LBNL) and Texas A&M (TAMU) (Task 3) that are designed capture complex coupled physical processes between flow and geomechanics, such as sand production, capillarity, and formation of secondary hydrates. The findings of Tasks 2 and 3 will be used to further improve numerical codes.

2) Develop (in Tasks 4 through 6) an advanced coupled geomechanics and non-isothermal flow simulator (T+M^{AM}) to account for large deformation and strong capillarity. This new code will be validated using data from the literature, from previous work by the project team, and with the results of the proposed experimental studies. The developed simulator will be applied to both Ulleung Basin and Prudhoe Bay sites, effectively addressing complex geomechanical and petrophysical changes induced by depressurization (e.g., frost-heave, strong capillarity, cryosuction, induced fracturing, and dynamic permeability).

Accomplished

The plan of the project timeline and tasks is shown in Table 1, and the activities and achievements during the third quarter of 2017 are listed as follows.

Task 1: Project management and planning

The second quarterly report was submitted, revised, and re-submitted to NETL. For Tasks 2, 4, and 5, Dr. Kim and his student visited KIGAM to have in-depth discussion with Drs. Lee and Ahn for the experimental results of Task 2.1 and 2.4, collecting the data. The data will be used for Task 4 and Subtask 5.2. For Task 3, the time lines between Subtasks 3.4 and 3.5 are swapped, and we have been performing Subtask 3.5, first. Table 1 shows the timelines of the project.

Task 2: Review and evaluation of experimental data of gas hydrate at various scales for gas production of Ullung Basin

We performed in-depth review for the experimental data of Subtasks 2.1 and 2.4, preparing the data for simulation, as follows.

Subtask 2.1 Evaluation of Gas hydrate depressurization experiment of 1-m scale

The experimental apparatus for the production test of gas hydrate (GH) have been used in cm-scale, typically. The cm-scale apparatus have limitations, such as the difficulty in getting an accurate production efficiency of GH on the variation of GH saturation due to the small quantity of in-situ GH in a specimen, difficulty of measuring propagation velocity of driving forces for GH production due to the short propagation distance of specimens, and difficulty of optical observation of specimen deformation and flow pattern in production well.

To overcome the limitations in cm-scale experimental apparatus, we developed meter-scale high pressure cell, and the system includes fluid/pressure control system, data acquisition system, temperature control system, and production control system to simulate GH production in sediment specimens. The cell can simulate flow phenomena during production only in uni-direction. In this study, we packed sediment sample into the meter-scale pressure cell. The packed sediments consisted of alternate layers of clay-sand-clay representing the layering system in the Ullung Basin geological structure. After forming GH, we investigated the production behavior of hydrate-bearing alternate layers of sand and mud under depressurization process

Experimental setup

The meter scale GH production system is composed of 4 major modules, which are meterscale high pressure cell, fluid control unit, data acquisition unit, and temperature control unit. Fig. 2.1 shows a picture of the system modules. The meter-scale high pressure cell made of 316 stainless steel was constructed with the working pressure of 20 MPa in order to simulate a hydrate reservoir. The dimensions of sediment specimens are 10 cm of the diameter and 100 cm of the length. Two K-type thermocouples for the temperature measurement at inlet and outlet and three K-Type multi-thermocouples for the internal temperature measurement of the specimen. Eleven Heise transducers and custom-made electrodes are equipped in every 10cm from the top end piece to the bottom for pressure and resistance measurements, respectively. Also, CCD cameras to visually monitor the surface of the specimen and 10 μm pore-sized filters to prevent intrusion of the soil particles into the flow line were installed at the upper and the lower end-caps.



Fig. 2.1. Picture of the experimental setup for 1D 1-m scale GH production

In injection module, two syringe pumps were used to inject water into the specimen and to control system pressure by dome-type back pressure regulator. Mass flow controllers were used to inject methane gas into the system. A wet test meter and a balance were used for the calculation of gas and water saturation change, respectively. We developed data acquisition module to control injection module and acquire the data including picture or videos of the sediment change using LabVIEW in real time, during the whole sequence of experiments.

The temperature of the most part of the system, especially the high pressure cell, was controlled using heat convection oven. The remaining parts related with fluid flows were insulated and their temperatures were controlled by circulating coolants. Heat exchanger was installed to prevent hydrate reformation in pipes outside of the cell, especially often occurred in back pressure regulator due to Joule-Thompson effect.

Experimental procedure

We used artificial sand that mimic the grain size distribution of sandy layers found in the Ulleung Basin, East Sea, Korea, as shown in Fig. 2.2. The dry sand-grains were slowly poured into the vibrated high pressure cell filled with water. After compaction, porosity and absolute permeability of the sand specimen saturated with water were measured. To establish initial water saturation, we injected methane gas into the specimen with constant flow rate. To minimize water flow in the specimens, methane injection rate was increased up to the highest flowing rate expected during production test. The system temperature was maintained at around 11°C.

Methane hydrate was formed at the initial water saturation from the specimen preparation step as following orders; pressurizing the cell by injecting methane, and cooled down system temperature from 11 to 2°C. An abrupt decrease in the fluid pressure indicated the hydrate formation.

The depressurization method was applied at the hydrate-bearing specimen to check the validity and applicability of the system. By controlling back pressure regulator, the fluid pressure of the cell was decreased from the stabilized pressure during GH formation to designated pressure, which is lower than equilibrium pressure at 2°C. The pressure, temperature, the volume of produced water and dissociated methane, and images of upper and lower specimen surfaces were recorded throughout the test.

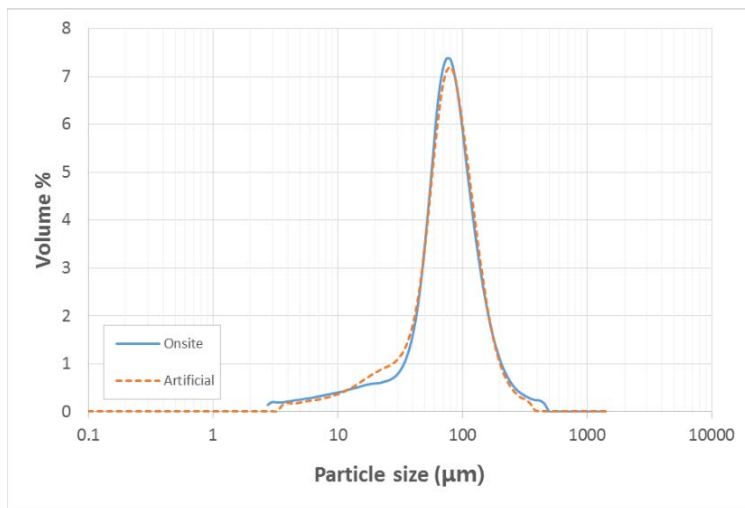


Fig. 2.2. Particle size distributions of onsite (Ulleung Basin) and artificial samples

Results

After GH formation, depressurization tests were conducted by decreasing system pressure down to 10, 20, 30, and 40% against the equilibrium pressure of methane hydrate at constant temperature condition. Fig. 2.3 illustrated the cumulative methane gas production of four test cases (DP 10%, DP 20%, DP 30%, and DP 40%). In this figure, the gas production was normalized to initial methane content in the cell. At all cases, normalized final gas production reached around 70% after the dissociation of GH. The cumulative production from 70 to around 90% was excluded in the calculation of recovery since it was due to the production of residual methane gas in the sediment pores by lowering the system pressure to the atmospheric pressure after the completion of depressurization. The result shows that the effect of depressurization level was insignificant on the final gas production volume.

Elapsed times to reach 70% gas recovery were compared in Fig. 2.4. The time of DP 20% was decreased drastically compared with that of DP 10% and the time differences between DP 20% and DP 40% were not significant. As expected, consumed time for the reaching final gas production shows exponential decrease pattern with increasing the level of depressurization.

In this study, we could not observe hydrate reformation phenomena. However this might be different in case of real field condition, such that the fluid system in the pore is composed of hydrate and water only and heat sources for the depressurization is limited. Because the hydrate reformation can cause severe reduction of production efficiency, it should be avoided or minimized in designing production method.

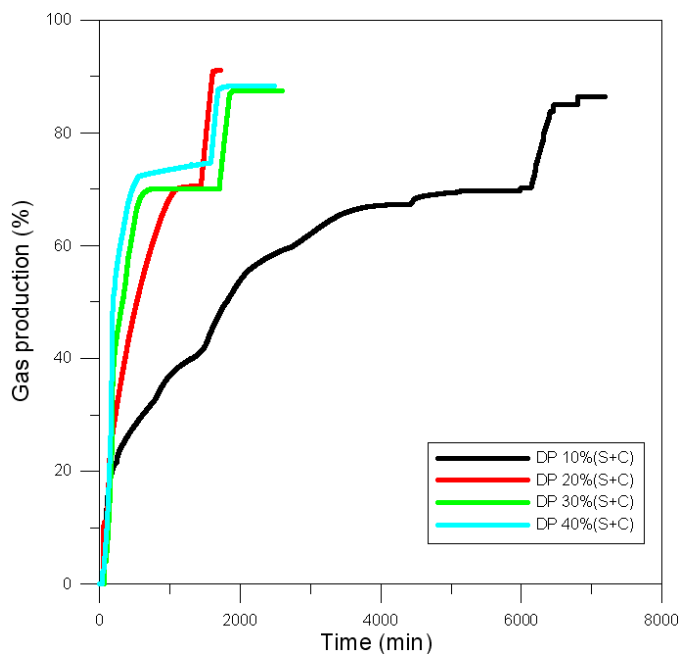


Fig. 2.3. Cumulative production profiles at four different depressurization cases

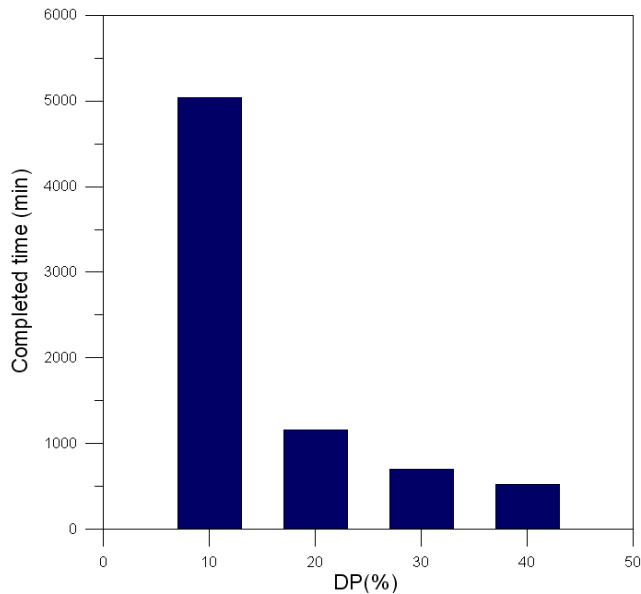


Fig. 2.4. Time to reach 70% gas recovery at four different depressurization cases

Subtask 2.2 Evaluation of Gas hydrate depressurization experiment of 10-m scale

Not initiated (future year tasks)

Subtask 2.3 Evaluation of Gas hydrate depressurization experiment of 1.5-m scale system in 3D

Not initiated (future year tasks)

Subtask 2.4 Evaluation of gas hydrate production experiment of the centimeter-scale system

For subtask 2.4, we revisited the experimental study on core-scale permeability measurements according to hydrate saturations, in order to make use of numerical simulation. In the experiment, we took specimens, choosing artificial samples and measuring porosity, of 98% SiO₂ of HAMA#5, 6, 7, 8 (grain density=2.68g/cm³, mean particle size 106~774 μm. Porosity of HAMA #5, 6, and 8 ranges from 0.39 to 0.40, while that of HAMA #7 is 0.43. We measured permeability with different hydrate saturation, ranging from 0.05 to 0.2 and pre-processed the data for numerical simulation

Specimens

Four different artificial sands (Hama #5, 6, 7, and 8) were used for the experiments. More than 98% of the sands are SiO₂ according to the XRF analyses. The grain density of sands were about 2.69g/cm³, according to the pycnometer measurements. The grain size distributions of four sands, measured by the laser diffraction particle analyzer are shown in Fig. 2.5. The mean particle sizes vary from 106 to 774 μm. The specimens were packed in cells with water pluviation methods in a vibrator. The initial porosity after specimens packing ranges from 0.39 to 0.43.

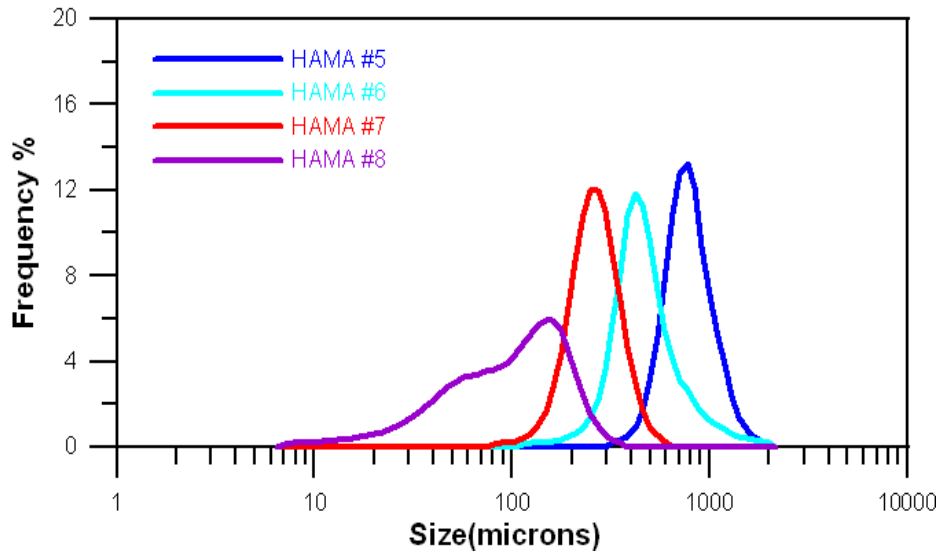


Fig. 2.5. Particle size distribution of the four sands

Experimental settings

A permeability measurement system that can maintain low temperature and high pressure for hydrate specimen were established. The system has four pressure vessels so that four experiments can be performed simultaneously. The system is largely comprised of four units: pressure vessels, the data acquisition unit, the flow and pressure control unit, and the temperature control unit (Fig. 2.6).

The working pressure of the pressure vessel is 3500 psia, and the inner dimension of the vessel is 2.54cm in diameter and 30cm in length. A cooling jacket is attached outside of each vessel and the temperatures of the pressure vessels were maintained by circulating fluid in the cooling jacket with refrigerating bath circulator.

The data acquisition unit has absolute pressure transducers that measure pressures from the top and bottom of a specimen, differential pressure transducers that measure differential pressures between the top and bottom of a specimen, and mass flow meters that measure the volume of the produced gas.

The flow and pressure control unit has mass flow controllers for controlled injection of gases, and a reciprocating pump for controlled water injections. The maximum flow rate for the mass flow controller is 1600sccm, and that of the reciprocating pump is 10ml/min.

The temperature control unit has refrigerating bath circulators connected to cooling jackets of pressure vessels.



Fig. 2.6. Permeability measurement system of hydrate-bearing sediments

Experimental procedures

After packing a specimen and assemble a pressure vessel, the temperature of a specimen was equilibrated at 11°C. The absolute water permeability of a specimen was measured by injecting water at several stages of flow rates. Methane gas was injected to a pre-determined initial water saturation and the specimen was pressurized with methane gas to about 700 psia. The temperature was lowered to 1°C to form hydrates in the specimen. Repressurizing the specimen with methane gas and forming hydrates were repeated until the pre-determined hydrate saturation was reached. After hydrate formation, effective permeability of methane gas was measured at several stages of flow rates. The permeability measurements were repeated four times per a specimen. After the effective permeability measurements, the hydrates in the specimens were dissociated by depressurization.

Results

The permeability as a function of hydrate saturation is plotted in Fig. 2.7. The permeability differences in same type of sand specimens with similar hydrate saturations could have been induced from heterogeneous character of hydrate formation in specimens. The effective permeability of methane gas in hydrate-bearing sediments tends to decrease with the increase of hydrate saturations and the decrease of mean grain sizes of specimens.

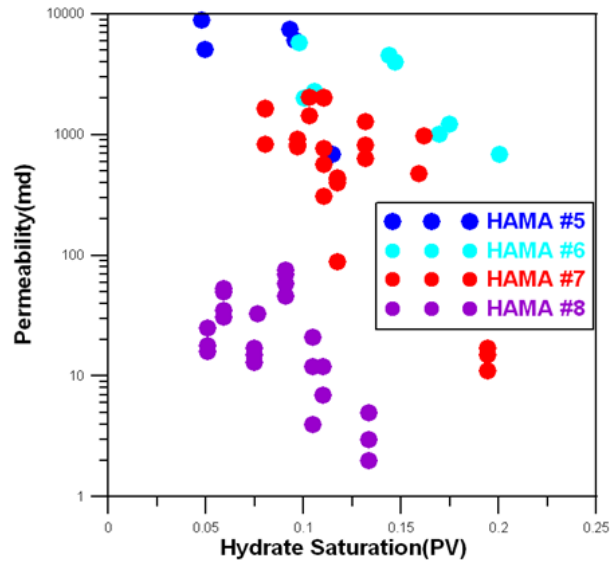


Fig. 2.7. Permeability versus hydrate saturation

Task 3: Laboratory Experiments for Numerical Model Verification

Subtask 3.1: Geomechanical changes from effective stress changes during dissociation

LBNL has been waiting for a larger X-ray transparent pressure vessel with multiple feed-throughs for this test. The vessel was ordered under another hydrate project in which it will be used as well, but is preferential to the existing vessel for these tests. The vessel was received this quarter and is being fitted with the needed plumbing (Figs. 3.1 and 3.2).



Fig. 3.1. New hydrate pressure vessel with thermal jacket and 2 end caps.

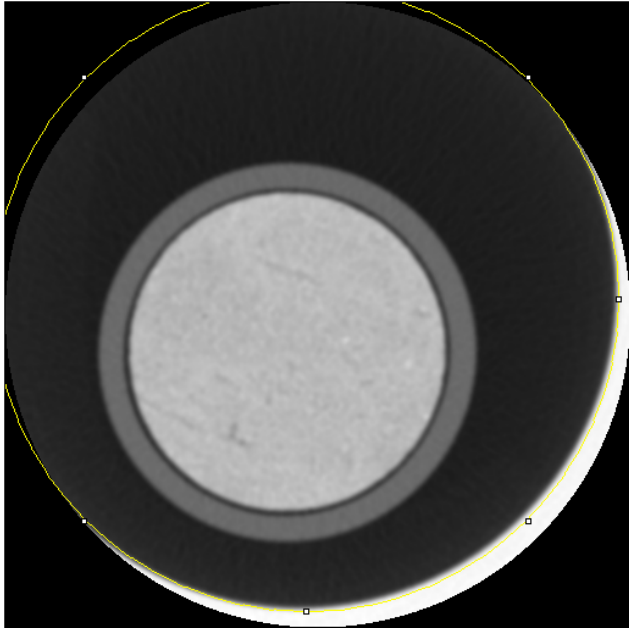


Fig. 3.2. Example of X-ray CT slice of Boise sandstone inside new vessel. The yellow circle has a 100 mm diameter.

Subtask 3.2 Geomechanical changes from effective stress changes during dissociation – sand
Production

Not initiated (future year tasks)

Subtask 3.3 Geomechanical changes resulting from secondary hydrate and capillary pressure
changes

Not initiated (future year tasks)

Subtask 3.4 Construction of the Relative Permeability Data in Presence of Hydrate

Not initiated (future year tasks)

Subtask 3.5 Identification of Hysteresis in Hydrate Stability

Experimental setup:

The experimental setup and the simulation model necessary for Subtask 3-5 have been described in earlier progress report. The measurement cylinder of the experiment is re-introduced in Fig. 3.3 in order to have completeness in the discussions of the new results. In the figure, note the location of the short, middle and long thermocouples placed inside the cylinder. These thermocouples are at 3.5 inches, 7.375 inches and 12.625 inches distance from the top, and the short and long thermocouples are placed near the wall, while the 7.375 inch thermocouple is placed at the center.

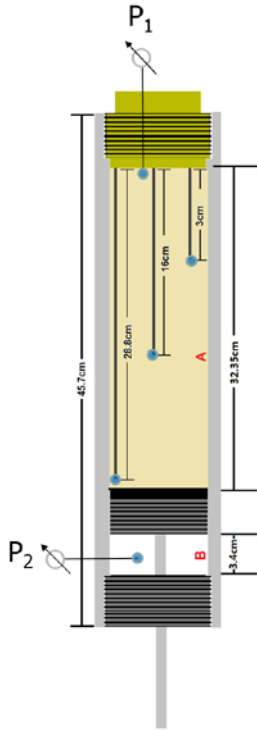


Fig. 3.3: Dissected diagram of the stainless steel cylinder to be used for Subtask 3.3 at Texas A&M University hydrate laboratory. The cylinder is placed inside of a refrigerator.

The procedure of the experiments performed are as follows: Stage 1 is the cooling and warming cycle of the cylinder when it is only filled with the distilled water; Stage 2 is the cooling and warming cycle of fully water saturated sand in the cylinder; and Stage 3 is the cooling and warming cycle of water and methane saturated sand in the cylinder. In essence, these stages are designed targeting a particular aspect of the hydrate study we target in Subtask 3-5. Stage 1, for example, is designed to analyze the heat transfer problem taking place inside the refrigerator and within the cylinder. Whereas Stages 1 and 2 help us understand the role of sand on the heat transfer. Stage 3, on the other hand, includes the effect of gas and hydrate. Clearly, as the number of stages is increased, the complexity of our problem is also increased but the analysis of the earlier stage help us control the level of complexity. The analyses involves simulation-based history matching of each stage of measurement. With each stage the difference between the stages will be known and that he effect is the addition of the next component and not a random effect or error. All measurements are repeated 3 times to show consistency and repeatability.

Stage 1: In this stage 1,200 ml of water is added to the hydrate cell and kept at 25 degrees Celsius to provide a consistent initial temperature point. Once the temperature has reached a point where the variation in the noise is less than a degree Celsius and there is no apparent slope in the last 40 minutes of data, the cooling cycle starts. The fridge is cooled to 1 degree Celsius and the fridge takes only a few minutes to reach the final temperature as seen in Fig. 3.4. As shown

in Fig. 3.4, there is an upper and lower bound, which is based on the 95 percentile confidence bounds, so the region of the overshoot is the largest source of error in the plot.

As mentioned earlier in the water-filled cylinder 3 thermocouples are placed. The response of each thermocouple is shown in Figs. 3.5-3.7. As can be seen there is little variation and the 95 percentile mark is very close to the averaged values of the readings except in a few areas, these areas are due to the variation in temperature of the fridge due to opening the door to the compressor room where the temperature of the room was suddenly reduced making the cooling more efficient for a while and then the door was shut, thus we see the shape of a squiggle. This is important later when the water responses are compared to the sand values, and any differences there can be attributed to the sand versus water, rather than error of the thermocouples.

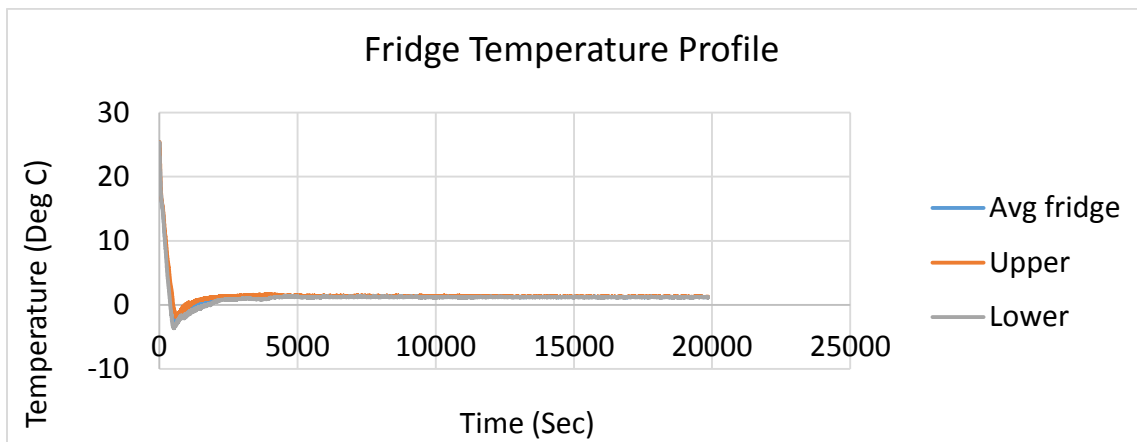


Fig. 3.4: Fridge Cooling Profile.

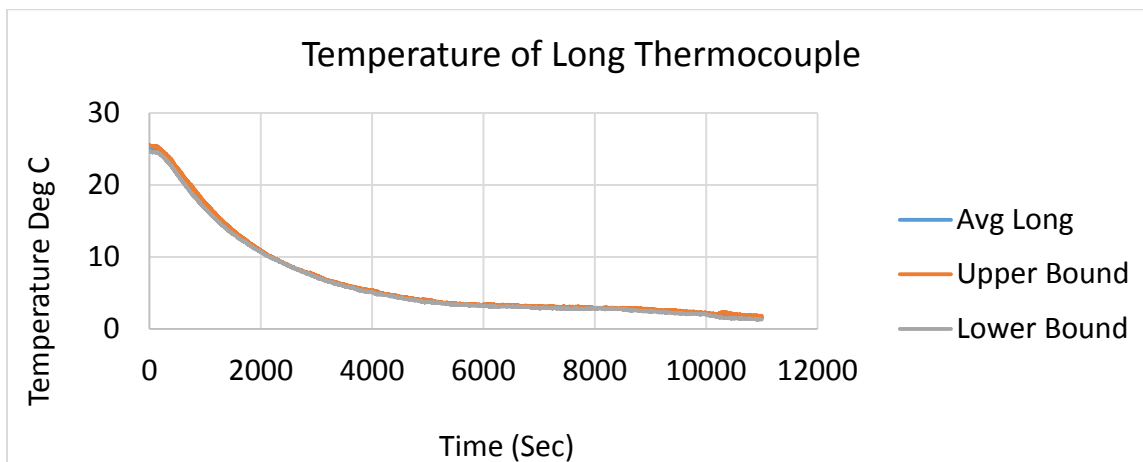


Fig. 3.5: Long thermocouple response to cooling in water only.

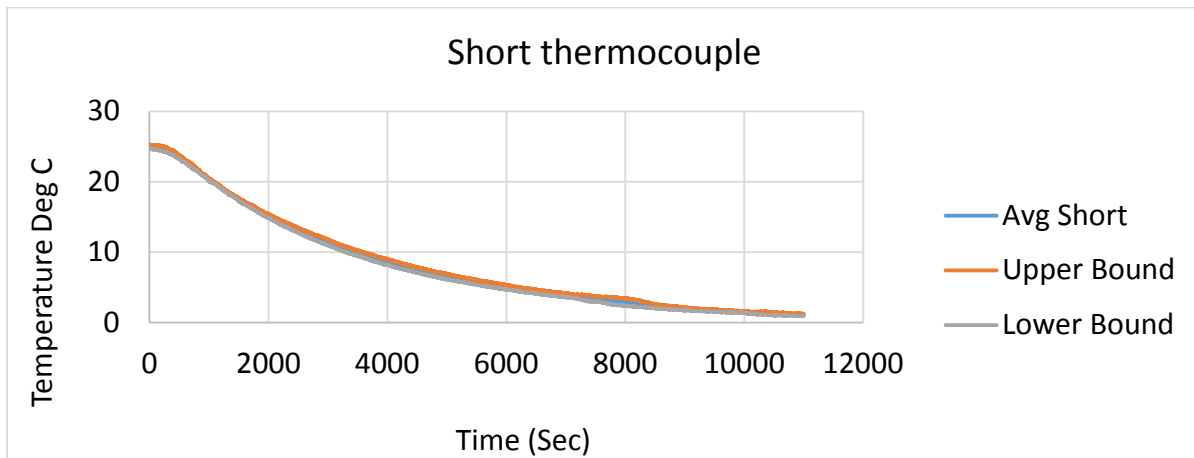


Fig. 3.6: Short thermocouple response to cooling in water only.

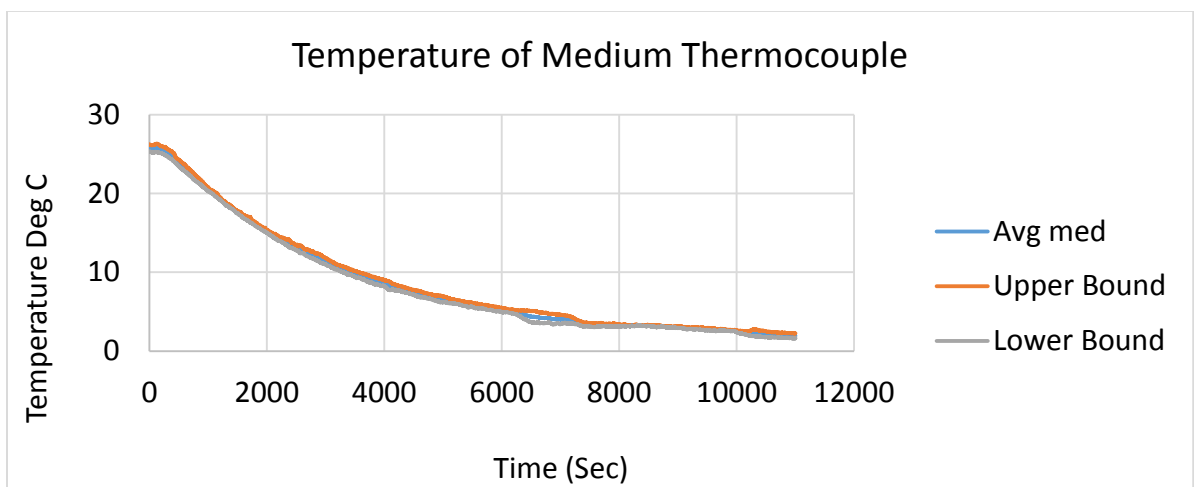


Fig. 3.7: Medium thermocouple response to cooling in water only.

Next, the heating profiles are presented in Figs. 3.8-3.11. It can be seen that the response is quite different than the cooling and while the fridge response was basically the same, the responses of the thermocouples show a nonlinear trend, but there is small confidence bounds so the results are satisfactory.

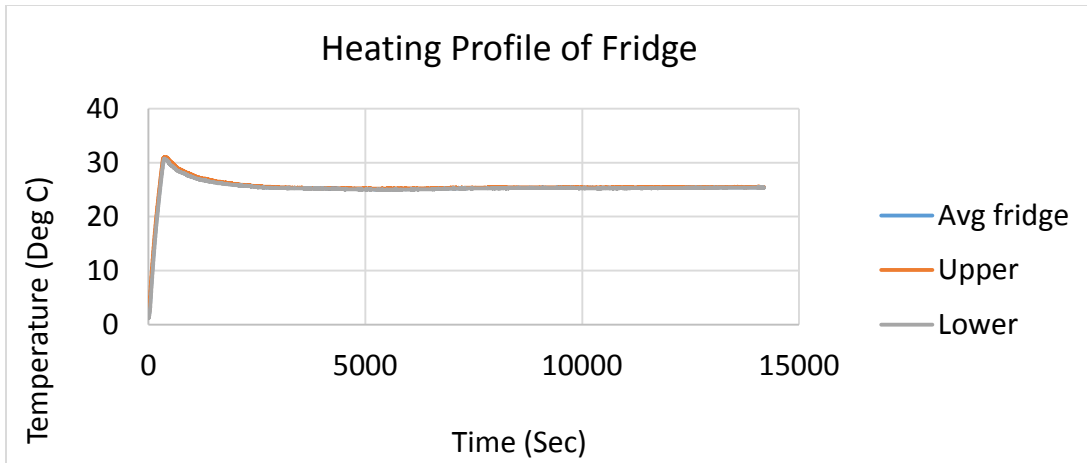


Fig. 3.8: Fridge heating profile

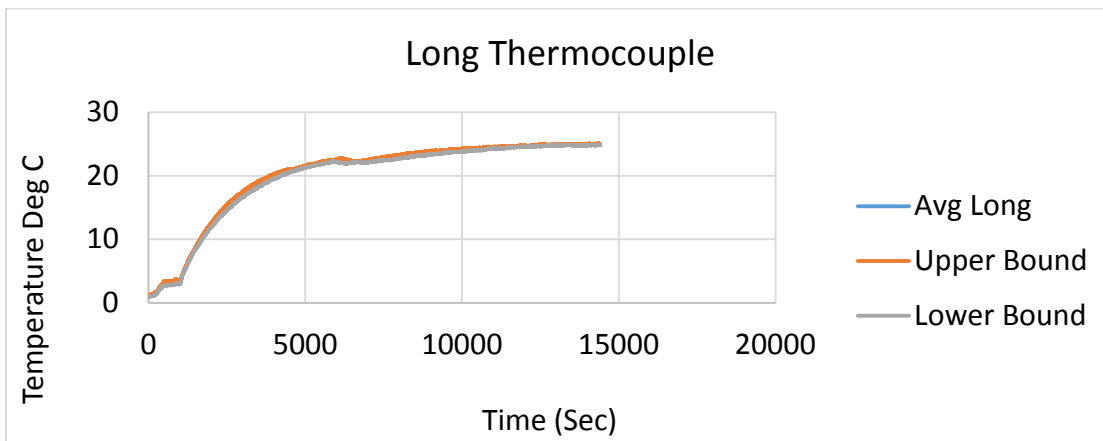


Fig. 3.9: Long thermocouple heating

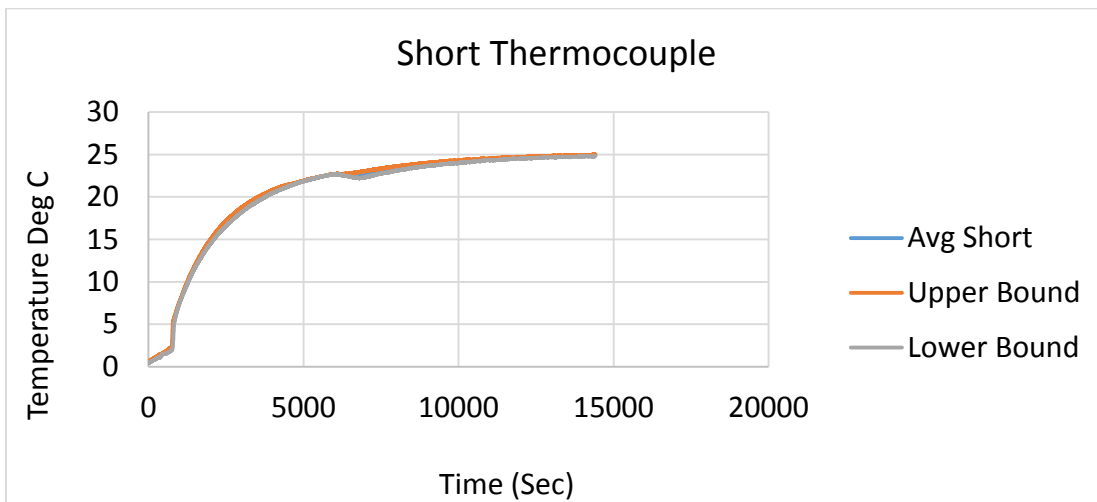


Fig. 3.10: Short thermocouple heating

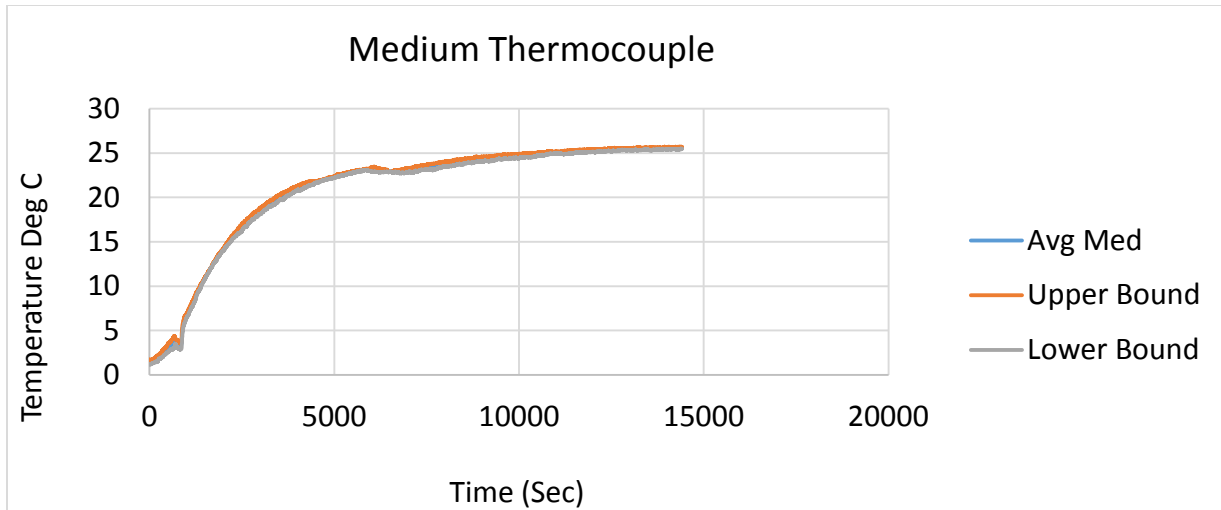


Fig. 3.11: Medium thermocouple heating

Stage 2: This stage of measurements consists of the cylinder filled with 1,200 ml of sand fully-saturated with water. The cell in the refrigerator is treated to the same temperature variations as in Stage 1. In Figs. 3.12-3.14 the responses to the same cooling profile as in Fig. 3.4 are shown. Notice that the temperature response of the system now is not nearly so nonlinear and the response of the thermocouples are smooth and accurate. The sand appears to dampen the nonlinearity in the cylinder's response and the boundary conditions are not as important. This is due to large volumetric heat capacity of the sand.

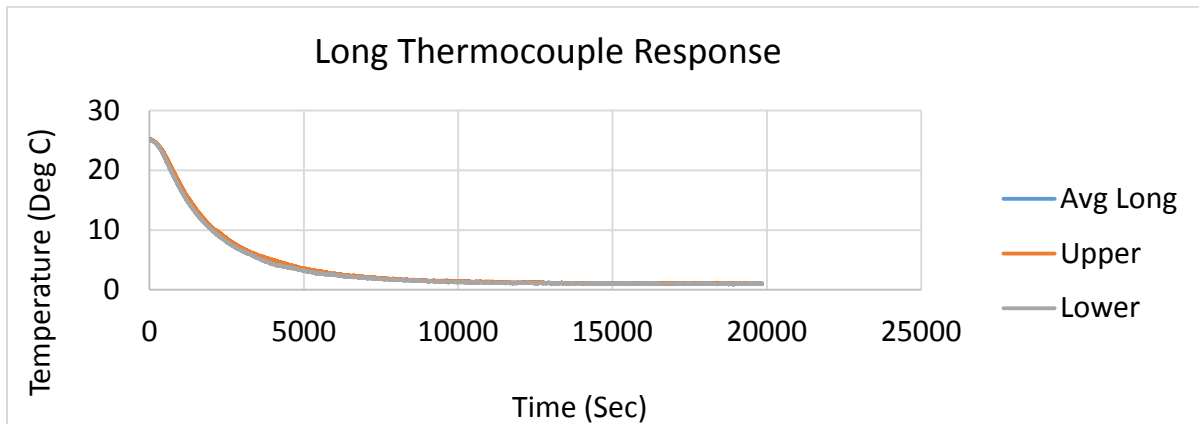


Fig. 3.12: Long thermocouple response in sand to cooling.

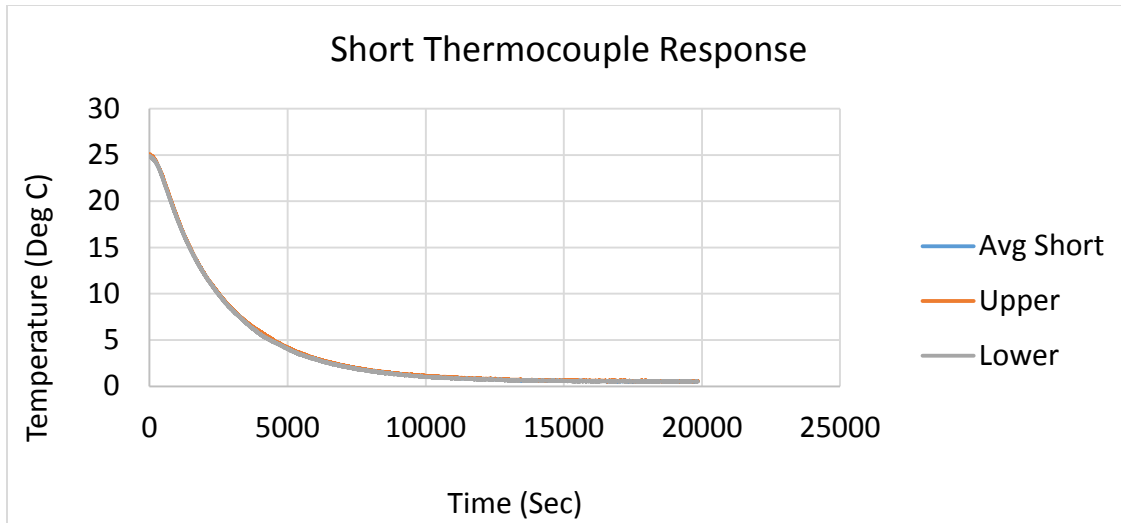


Fig. 3.13: Short thermocouple response in sand to cooling.

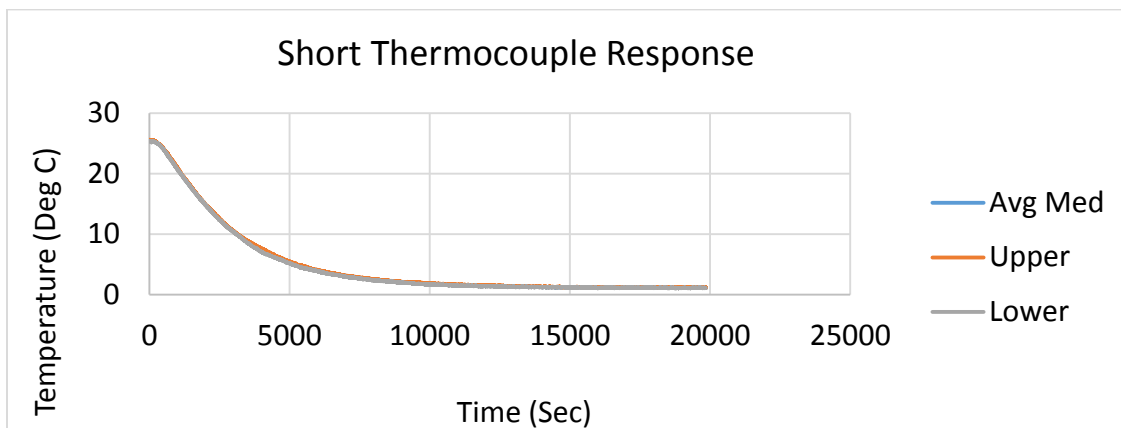


Fig. 3.14: Medium thermocouple response in sand to cooling.

In Figs. 3.15-3.18 the temperature history of the heating cycle is shown. As in Stage 1 the errors are larger and the heating profile of the fridge are the same as in Fig. 3.8. The response is still nonlinear for the heating of the sand with water, thus there is some mechanical effect that is preventing the sand water mixture to respond smoothly when compared to the cooling. In Fig.18 the nonlinear effects appear when the temperature difference between the fridge and the sand are small. Within the first 4,000 seconds the fridge temperature has leveled out and the sand temperatures are smooth, but around the 6,000 mark there is a significant decrease in temperature even though there is a slight increase in the fridge temperature. Furthermore, the response is not seen in the long thermocouple, but these are also the areas where there is the greatest uncertainty, thus more experiments is needed to see if this phenomenon persists.

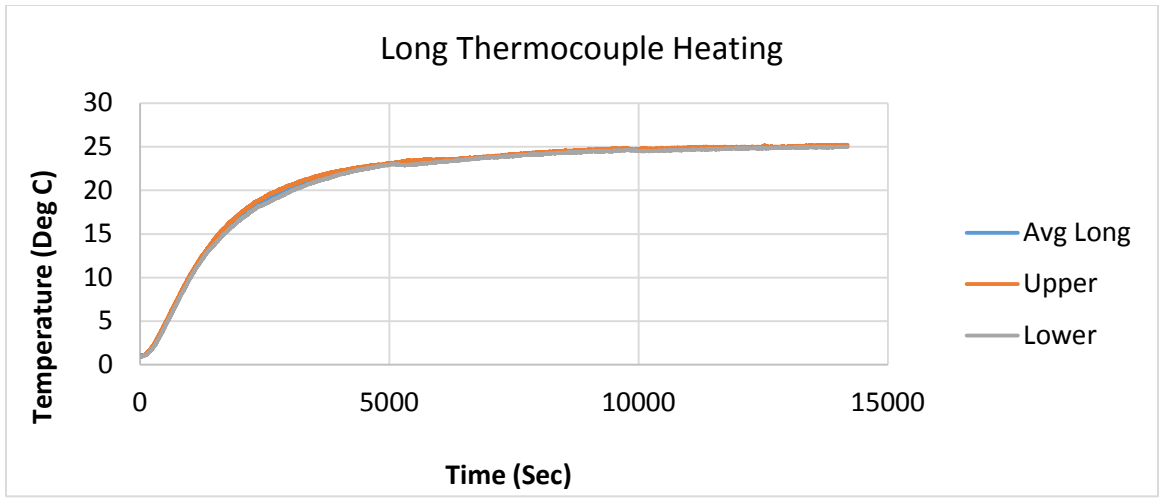


Fig. 3.15: Long thermocouple response in sand to heating

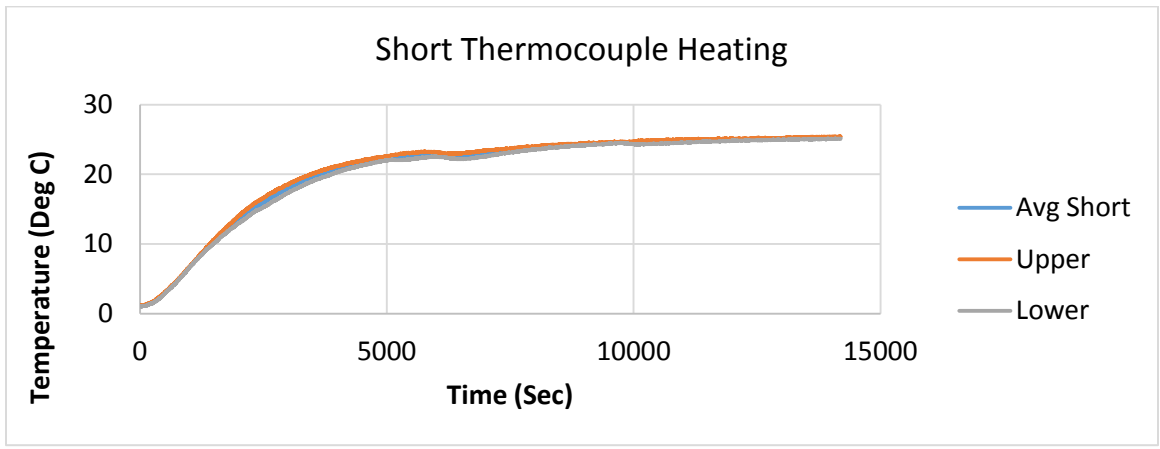


Fig. 3.16: Short Thermocouple response in sand to heating

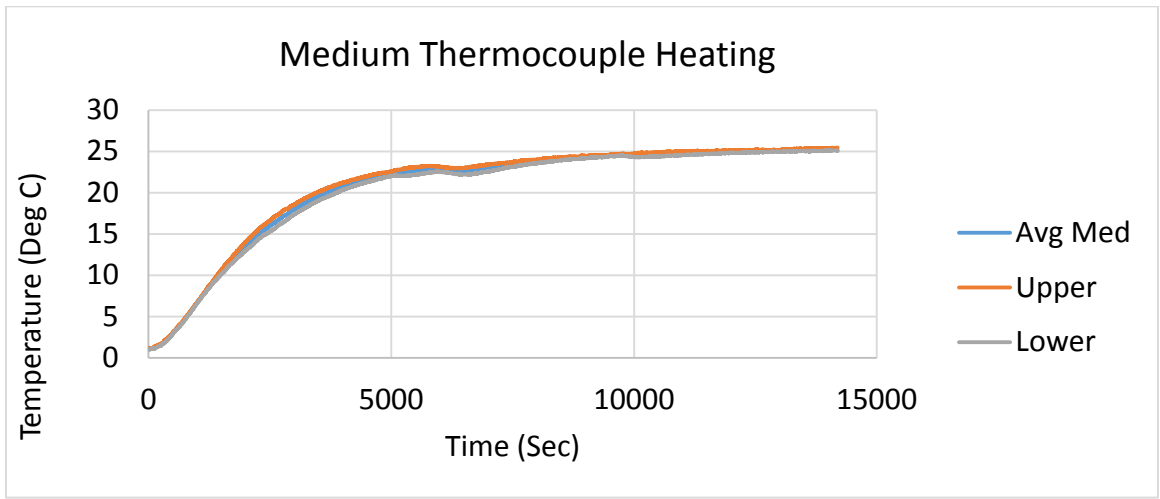


Fig. 3.17: Medium Thermocouple response in sand to heating.

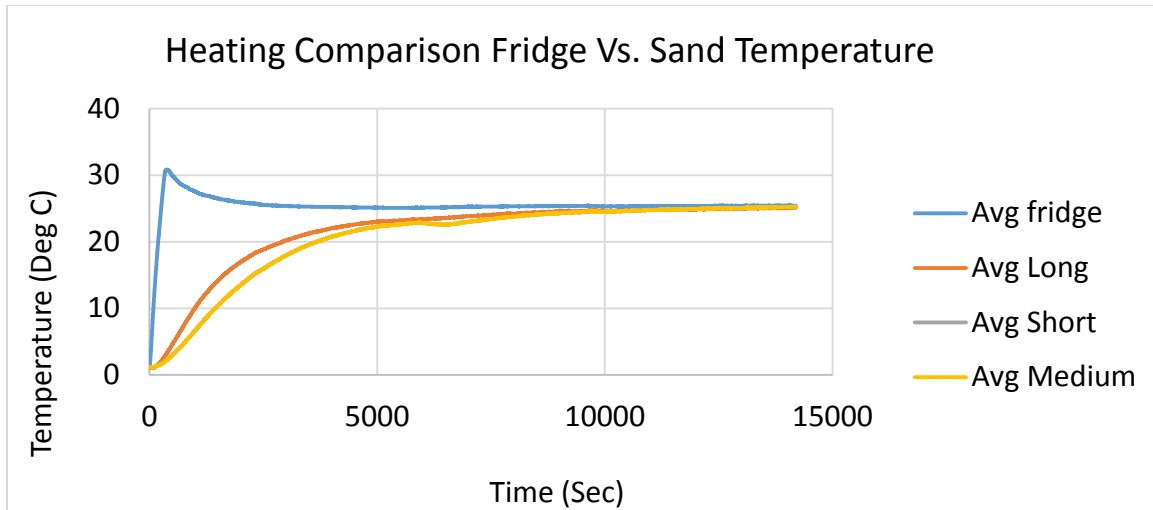


Fig. 3.18: Comparison of thermocouple responses to fridge heating profile.

The next step is to compare the differences of the water and sand+water runs to show that there is a marked difference in between the two cases. In Figs. 3.19-3.21 we show the response during cooling and in Figs. 3.22-3.24 we show the differences during heating. In the water only case during the cooling, the water takes longer than the sand to cool by a good margin, but notice that this is only after the cooling of the fridge has leveled out and that the temperature difference between the fridge and the thermocouples has significantly reduced. This is only true for the long and short thermocouples as the medium one has the largest difference for most of the time during the cooling.

The same trend is also observed in the heating profiles where the water saturated sand is much more conductive than the water only case. And the nonlinearity of the water only case is clear. There are places where the temperature levels off for a while and even decreases, while in the sand case this is not seen.

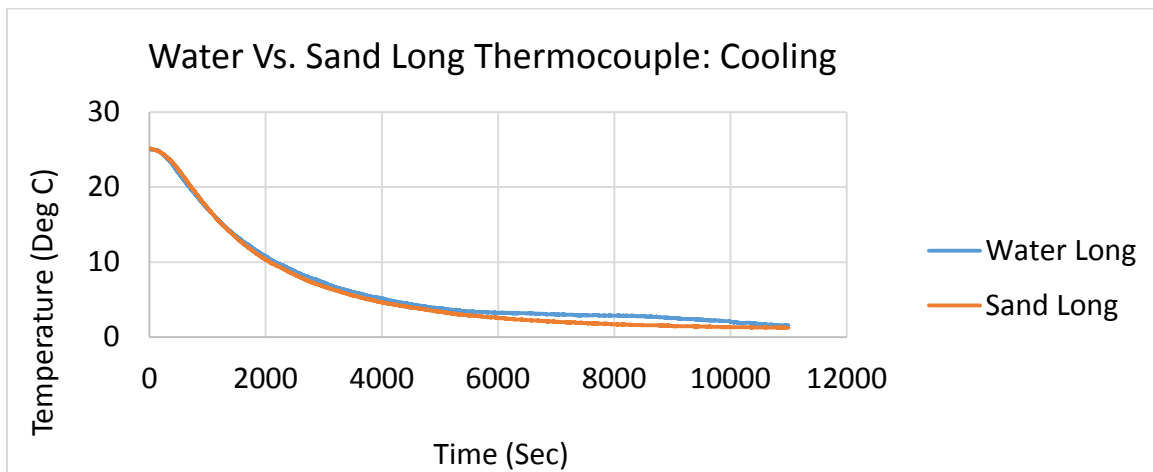


Fig. 3.19: Long Thermocouple response to cooling, for water only, and fully saturated sand.

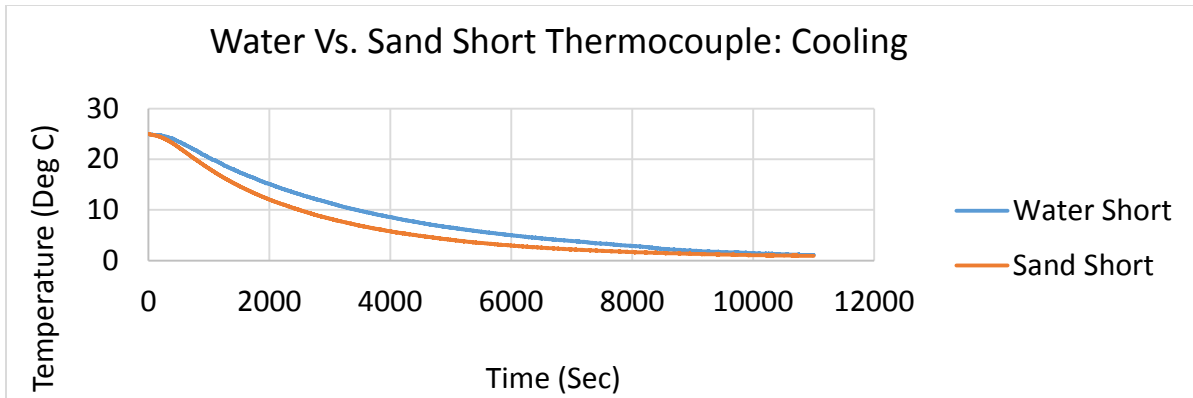


Fig. 3.20: Short thermocouple response to cooling, for water only, and fully saturated sand.

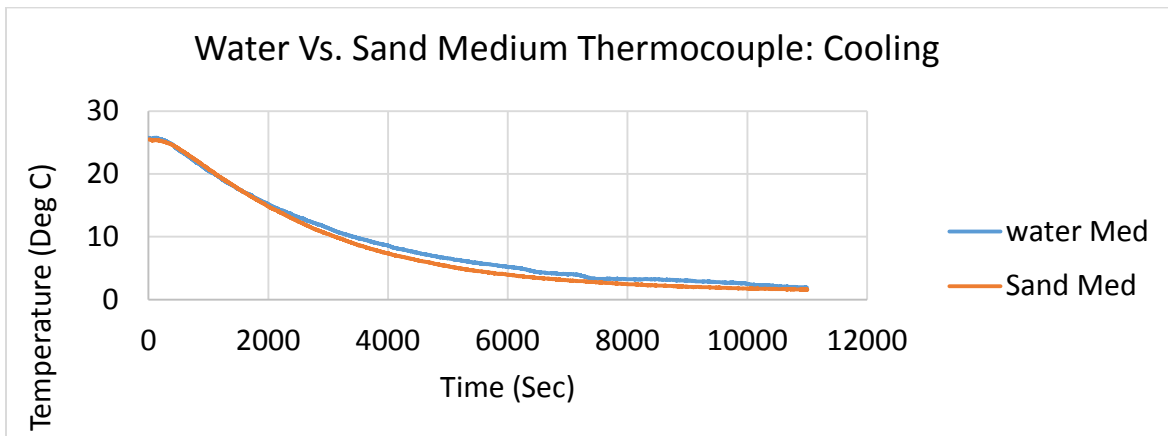


Fig. 3.21: Medium Thermocouple responses to cooling, for water only, and fully saturated sand.

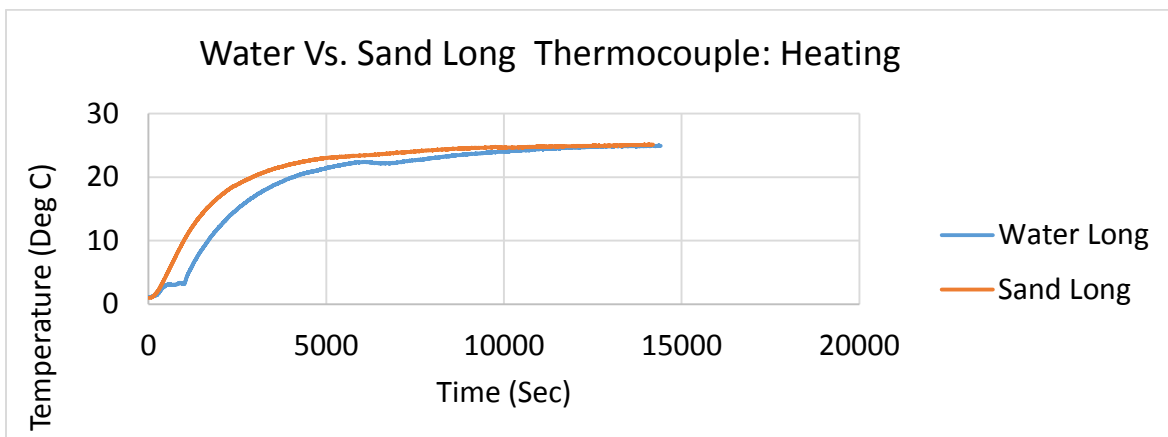


Fig. 3.22: Long Thermocouple response to heating, for water only, and fully saturated sand.

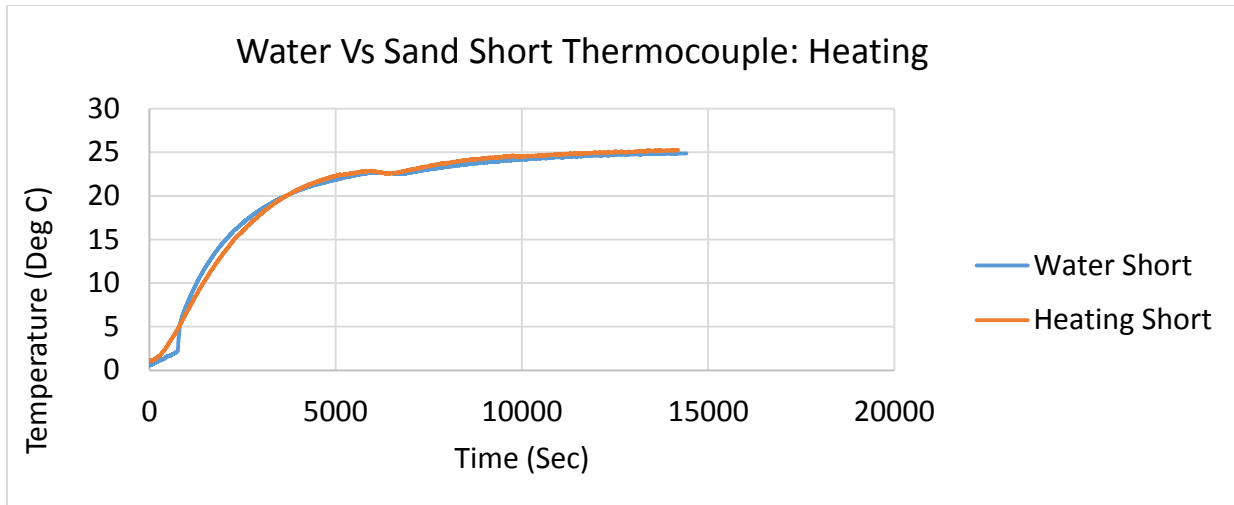


Fig. 3.23: Short thermocouple response to heating, for water only, and fully saturated sand.

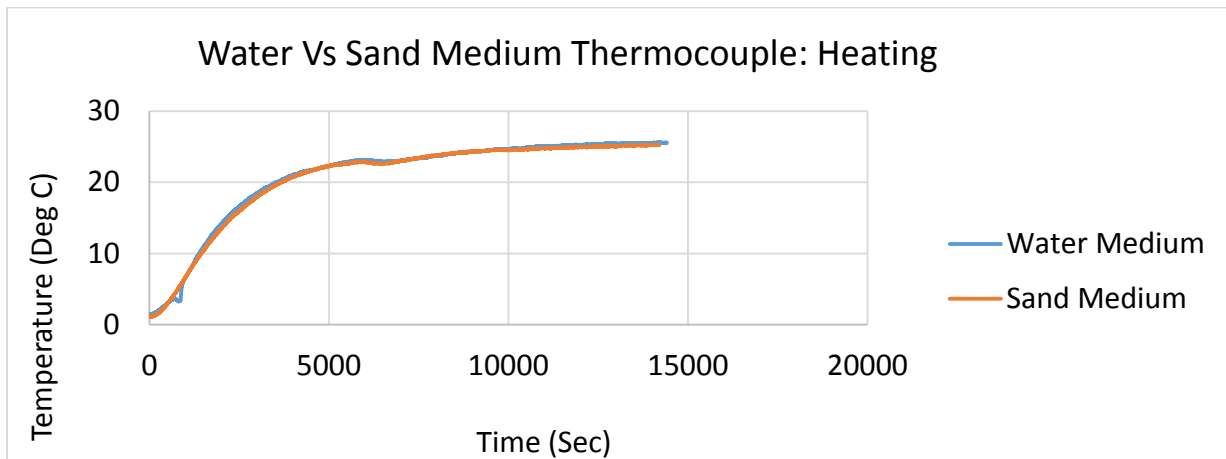


Fig. 3.24: Medium thermocouple response to heating, for water only, and fully saturated sand.

Stage 3

This stage is the same as the previous case but now the cylinder includes the combination of sand water and gas. The sand filled cylinder now holds a 50/50 percent saturation of water to gas. We perform the cooling and heating cycles after the fluids are gravity-stabilized, hence the flow effects associated with the upward migration of the gas phase has already taken place prior to the beginning of the measurements. The response has some interesting new effects where one observes that there is an increase in temperature at the point of hydrate formation as shown in Fig. 3.25.

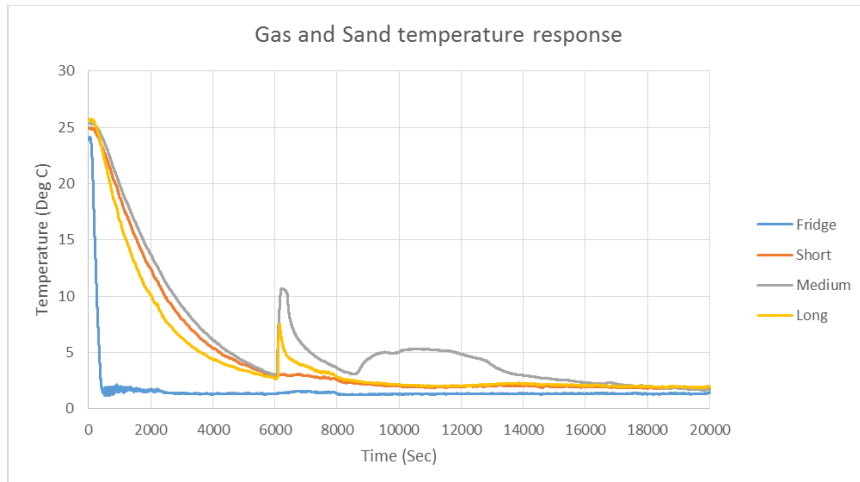


Fig. 3.25: Sand and gas and water temperature profile

Work to be done:

In our earlier progress report, we have already introduced the simulation part of the work. The next step in our investigation is to use simulation to history match the trends presented at each stage and proceed into the intricacies of the hydrate formation in the cylinder. We anticipate that Task 3-5 will be completed in Fall 2017.

Task 4: Incorporation of Laboratory Data into Numerical Simulation Model

Subtask 4.1 Inputs and Preliminary Scoping Calculations

Not initiated (future year tasks)

Subtask 4.2 Determination of New Constitutive Relationships

Continuing to the previous progress, we are currently updating TOUGH+Hydrate, implementing the hysteresis subroutines, as shown in Hyun et al (2017), SPE182709.

Subtask 4.3 Development of Geological Model

Not initiated (future research work)

Task 5: Modeling of coupled flow and geomechanics in gas hydrate deposits

Subtask 5.1 Development of a coupled flow and geomechanics simulator for large deformation

Continuing to the previous progress in 2D, we are completing full 3D and 2D axisymmetric coupled flow and largely deformable geomechanics simulators, respectively. In particular, we have made the 2D axisymmetric geomechanics codes for Subtasks 5.2.

Subtask 5.2 Validation with experimental tests of depressurization

We have initiated this task, completing the 2D axisymmetric geomechanics codes for infinitesimal transformation (small deformation) as well as large deformation. Note that all the experimental tests are based on cylindrical samples. As addressed in the 9th International Conference on Gas Hydrates (ICGH), the existing 2D plane strain geomechanics is hardly applied to the physical problems that have cylindrical coordinates because of numerical instability near the wellbore (depressurization area). The 2D axisymmetric geomechanics codes were easily implemented with minor modification of the 2D plane-strain geomechanics codes for both small and large deformation.

Before the validation tests, we verified the axisymmetric geomechanics codes with analytical solutions. Specifically, Fig. 5.1 shows comparison between numerical results and the analytical solutions for small deformation. We used an irregular mesh (21*21), where the horizontal grid sizes are 0.01m, 0.09m, 0.9m, 1m, 2m, 4m, 8m, and 10m of the rest 14 gridblocks. The vertical grid sizes are uniform (1m). Even though we had very fine gridblocks near the well, we identified that the numerical results matched the analytical solutions.

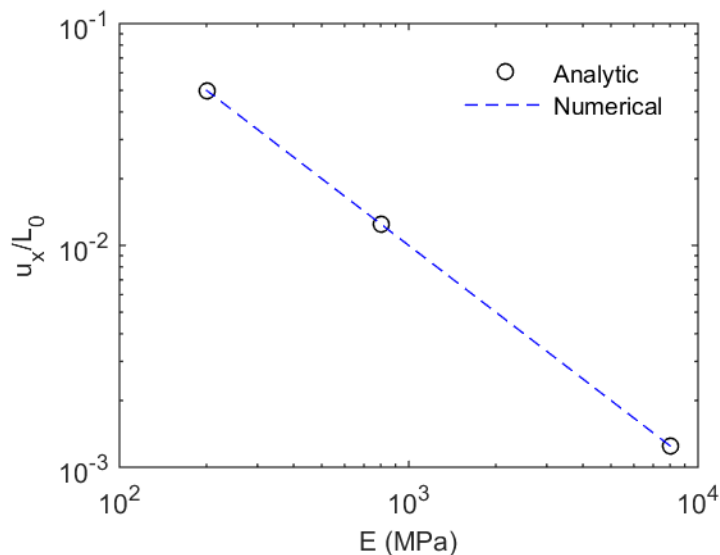


Fig. 5.1 Comparison between numerical and analytical solutions for axisymmetric geomechanics.

Subtask 5.3 Modeling of sand production and plastic behavior

Not initiated (future task).

Subtask 5.4 Modeling of induced changes by formation of secondary hydrates: Frost-heave, strong capillarity, and induced fracturing

Continuing the previous research on induced fracturing, we have made the draft of the manual of the 2D non-planar fracture propagation simulator. Note that the computer code is based on the finite element method with the cohesive zone model. The manual almost follows the format of the manuals of TOUGH family codes. Currently, we are coupling TOUGH+Hydrate (flow simulator) to this fracture propagation simulator.

Subtasks 5.5 and 5.6 Field-scale simulation of PBU L106 and Ulleung Basin

Along with the 3D parallel simulation of geomechanics, we have been reviewing the previous simulation results of PBU L106 and Ulleung Basin. We have purchased a multi-core computer and FLAC3D. We are re-visiting the simulations of PBU L106-C unit and Ulleung Basin, which were studied with FLAC3D in 2012 and 2013, respectively.

Task 6: Simulation-Based Analysis of System Behavior at the Ignik-Sikumi and Ulleung Hydrate Deposits

We have trained thoroughly a TAMU student in the use and application of the Tough+Hydrate code. The training lasted all spring semester. We are now building the grid for a very complex laboratory experiment that is part of the TAMU activities. Note that the LBNL simulation role is in training and advising, and TAMU students execute.

PRODUCTS

We participated in the 9th International Conference on Gas Hydrates (ICGH), Denver, Colorado, June 25-30, having presentations, as follows.

Kim, J., Lee, J.Y., 2017, Rigorous simulation of coupled non-isothermal flow and largely deformable geomechanics for gas hydrate deposits.

Ahn, T., Lee, J., Lee, J.Y., Kim, S.J., Seo, Y.J., 2017 Depressurization-induced production behavior of methane hydrate in a meter-scale alternate layer of sand and mud.

BUDGETARY INFORMATION

Table 2 shows the information of the budget for this project and the expenditure up to 06/30/2017. The expenses in LBNL to date are still zero, and we believe that the account number did not get transferred to the appropriate location. This problem is being investigated.

Table 1 – Project timeline and milestones (Gantt Chart)

	FY17				FY18				FY19			
Quarter	Q1	Q2	Q3	Q4	Q1	Q2	Q3	Q4	Q1	Q2	Q3	Q4
Task 1.0. Project Management/Planning	A											
Task 2.0. Experimental study of gas hydrate in various scales for gas production of Ulleung Basin												
<i>Subtask 2.1. Depressurization of 1 m scale in 1D</i>				B								
<i>Subtask 2.2. Depressurization of 10-m scale in 1D</i>							C					
<i>Subtask 2.3. Depressurization of 1.5-m scale in 3D</i>										D		
<i>Subtask 2.4. Revisit to the centimeter-scale system</i>												
Task 3.0. Laboratory Experiments for Numerical Model Verification												
<i>Subtask 3.1. Effective stress changes during dissociation</i>				E								
<i>Subtask 3.2. Sand production</i>								F				
<i>Subtask 3.3. Secondary hydrate and capillary pressure changes</i>												G
<i>Subtask 3.4. Relative Permeability Data</i>												
<i>Subtask 3.5. Hysteresis in Hydrate Stability</i>												
Task 4.0. Incorporation of Laboratory Data into Numerical Simulation Model												
<i>Subtask 4.1. Inputs and Preliminary Scoping Calculations</i>										H		
<i>Subtask 4.2. Determination of New Constitutive Relationships</i>												
<i>Subtask 4.3. Development of Geological Model</i>												
Task 5.0. Modeling of coupled flow and geomechanics in gas hydrate deposits												
<i>Subtask 5.1. Development of a coupled flow and geomechanics simulator for large deformation</i>				I								
<i>Subtask 5.2. Validation with experimental tests of depressurization</i>										J		
<i>Subtask 5.3. Modeling of sand production and plastic behavior</i>								K				
<i>Subtask 5.4. Frost-heave, strong capillarity, and induced fracturing</i>												L
<i>Subtask 5.5. Field-scale simulation of PBU L106</i>												
<i>Subtask 5.6. Field-wide simulation of Ulleung Basin</i>												
Task 6.0. Simulation-Based Analysis of System Behavior at the Ignik-Sikumi and Ulleung Hydrate Deposits												M

Table 2 Budget information

Baseline Reporting Quarter	Budget Period 1							
	Q1		Q2		Q3		Q4	
	10/01/16-12/31/16		01/01/17-03/31/17		04/01/17-06/30/17		07/01/17-09/30/17	
	Q1	Cumulative Total	Q2	Cumulative Total	Q3	Cumulative Total	Q4	Cumulative Total
Baseline Cost Plan								
Federal (TAMU)	\$37,901	\$37,901	\$57,809	\$95,711	\$43,967	\$139,678	\$34,206	\$173,884
Federal (LBNL)	\$18,750	\$18,750	\$18,750	\$37,500	\$18,750	\$56,250	\$18,750	\$75,000
Non-Federal Cost Share	\$6,986	\$6,986	\$6,986	\$13,972	\$6,986	\$20,958	\$656,986	\$677,944
Total Planned	\$63,637	\$63,637	\$83,545	\$147,183	\$69,703	\$216,886	\$709,942	\$926,828
Actual Incurred Cost								
Federal (TAMU)	\$0	\$0	\$10,235	\$10,235	\$57,085	\$67,321		
Federal (LBNL)	\$0	\$0	\$0	\$0	\$0	\$0		
Non-Federal Cost Share	\$0	\$0	\$6,986	\$6,986	\$6,986	\$13,972		
Total incurred cost	\$0	\$0	\$17,221	\$17,221	\$64,071	\$81,293		
Variance								
Federal (TAMU)	(\$37,901)	(\$37,901)	(\$47,574)	(\$85,475)	\$13,118	(\$72,357)		
Federal (LBNL)	(\$18,750)	(\$18,750)	(\$18,750)	(\$37,500)	(\$18,750)	(\$56,250)		
Non-Federal Cost Share	(\$6,986)	(\$6,986)	\$0	(\$6,986)	\$0	(\$6,986)		
Total variance	(\$63,637)	(\$63,637)	(\$66,324)	(\$129,961)	(\$5,632)	(\$135,593)		

Baseline Reporting Quarter	Budget Period 2							
	Q1		Q2		Q3		Q4	
	10/01/17-12/31/17		01/01/18-03/31/18		04/01/18-06/30/18		07/01/18-09/30/18	
	Q1	Cumulative Total	Q2	Cumulative Total	Q3	Cumulative Total	Q4	Cumulative Total
Baseline Cost Plan								
Federal (TAMU)	\$42,481	\$42,481	\$35,307	\$77,788	\$46,367	\$124,155	\$39,908	\$164,063
Federal (LBNL)	\$18,750	\$18,750	\$18,750	\$37,500	\$18,750	\$56,250	\$18,750	\$75,000
Non-Federal Cost Share	\$6,986	\$6,986	\$6,986	\$13,972	\$6,986	\$20,958	\$6,986	\$27,944
Total Planned	\$68,217	\$68,217	\$61,043	\$129,260	\$72,103	\$201,363	\$65,644	\$267,007
Actual Incurred Cost								
Federal (TAMU)								
Federal (LBNL)								
Non-Federal Cost Share								
Total incurred cost								
Variance								
Federal (TAMU)								
Federal (LBNL)								
Non-Federal Cost Share								
Total variance								

Baseline Reporting Quarter	Budget Period 3							
	Q1		Q2		Q3		Q4	
	10/01/18-12/31/18		01/01/19-03/31/19		04/01/19-06/30/19		07/01/19-09/30/19	
	Q1	Cumulative Total	Q2	Cumulative Total	Q3	Cumulative Total	Q4	Cumulative Total
Baseline Cost Plan								
Federal (TAMU)	\$43,543	\$43,543	\$36,189	\$79,733	\$47,526	\$127,259	\$41,209	\$168,468
Federal (LBNL)	\$18,750	\$18,750	\$18,750	\$37,500	\$18,750	\$56,250	\$18,750	\$75,000
Non-Federal Cost Share	\$6,986	\$6,986	\$6,986	\$13,972	\$6,986	\$20,958	\$6,986	\$27,944
Total Planned	\$69,279	\$69,279	\$61,925	\$131,205	\$73,262	\$204,467	\$66,945	\$271,412
Actual Incurred Cost								
Federal (TAMU)								
Federal (LBNL)								
Non-Federal Cost Share								
Total incurred cost								
Variance								
Federal (TAMU)								
Federal (LBNL)								
Non-Federal Cost Share								
Total variance								

National Energy Technology Laboratory

626 Cochrans Mill Road
P.O. Box 10940
Pittsburgh, PA 15236-0940

3610 Collins Ferry Road
P.O. Box 880
Morgantown, WV 26507-0880

13131 Dairy Ashford Road, Suite 225
Sugar Land, TX 77478

1450 Queen Avenue SW
Albany, OR 97321-2198

Arctic Energy Office
420 L Street, Suite 305
Anchorage, AK 99501

Visit the NETL website at:
www.netl.doe.gov

Customer Service Line:
1-800-553-7681



U.S. DEPARTMENT OF
ENERGY

**NATIONAL ENERGY
TECHNOLOGY LABORATORY**